The Post-reionization neutral IGM : A Cosmological Probe

TAPOMOY GUHA SARKAR

Birla Institute of Technology and Science
Pilani, India.

COSMOLOGY DAY
ICTS Bangalore
8th April 2014

POST REIONIZATION EPOCH

Following the completion of reionization (z~6), HI was confined to over-dense regions of the IGM where enhanced recombination maintains a non-zero neutral fraction

80% of HI is in DLA systems

$\Omega_{\rm HI} \sim 10^{-3}$ (Prochaska, Herbert-Fort & Wolfe 2005)

The Post reionization HI can be studied using 21 cm intensity maps

Aim of several presently functioning and upcoming Radio-Telescopes GMRT, MWA, SKA

HI from the same z can be seen through
Redshifted 21 cm line EMISSION or through
ABSORBTION features in Quasar spectra
(Lyman-α forest)

The signals have different origins –
The Lyman-α forest originate from small HI fluctuations in the primarily ionized IGM. 21 cm radiation from these regions is negligible.

The 21 cm radiation originates primarily from the self shielded and dense DLA systems which contain most of the neutral gas.

On large scales however they both trace the underlying Dark Matter distribution and hence expected to be correlated

The Post Reionization HI:

Two astrophysical systems of interest :

Lyman-α Forest:

Optically Thin Ly-α absorbers $N(HI) < 10^{17}\ cm^{-2}$ in a primarily ionized IGM .

DLA Systems:

Dense, self shielded, Neutral. $N(HI) > 10^{19}\ cm^{-2}$
with $\tau \sim 1$, in the damping wings.
Line width independent of the gas velocity structure.
~ 80% of the HI at $z < 4$ is contained in DLAs.

Equilibrium between the UV background ionizing and Recombination rate at local gas density maintains ionizing fraction.

HI 21 cm observations as a COSMOLOGICAL PROBE

- **Galaxy/quasar redshift surveys can't probe the universe at very high redshifts, with the potential to probe large volumes.**
- **CMB photons free streaming from the LSS Undergoes a dip in its brightness temperature on passing through a HI cloud depending on its optical depth and spin temperature .**
- **The spatial fluctuations of this "dip" depends directly and indirectly on the fluctuations of the HI which in turn follows the underlying dark matter**

21-cm INTENSITY MAPPING : LARGE SURVEY VOLUMES AND LOW RESOLUTION MAPPING

HI 21 cm observations as a COSMOLOGICAL PROBE

- **Galaxy /quasar redshift surveys can't probe the universe at very high redshifts, with the potential to probe large volumes.**
- **CMB photons free streaming from the LSS Undergoes a dip in its brightness temperature on passing through a HI cloud depending on its optical depth and spin temperature .**
- **The spatial fluctuations of this "dip" depends directly and indirectly on the fluctuations of the HI which in turn follows the underlying dark matter**

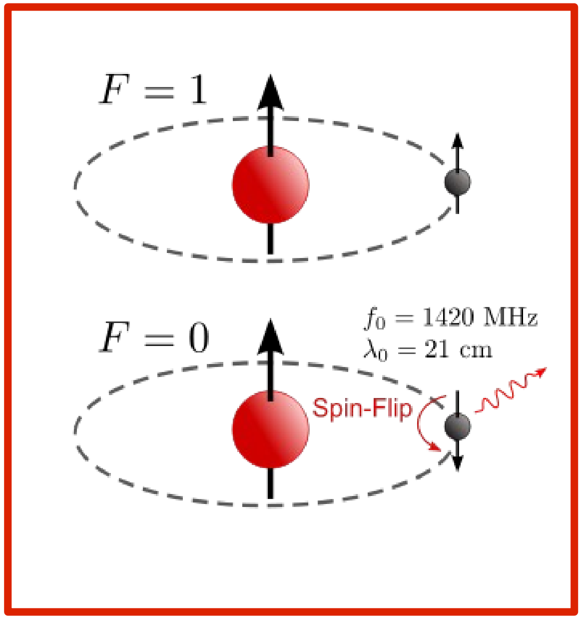

(Bharadwaj and Ali 2004)

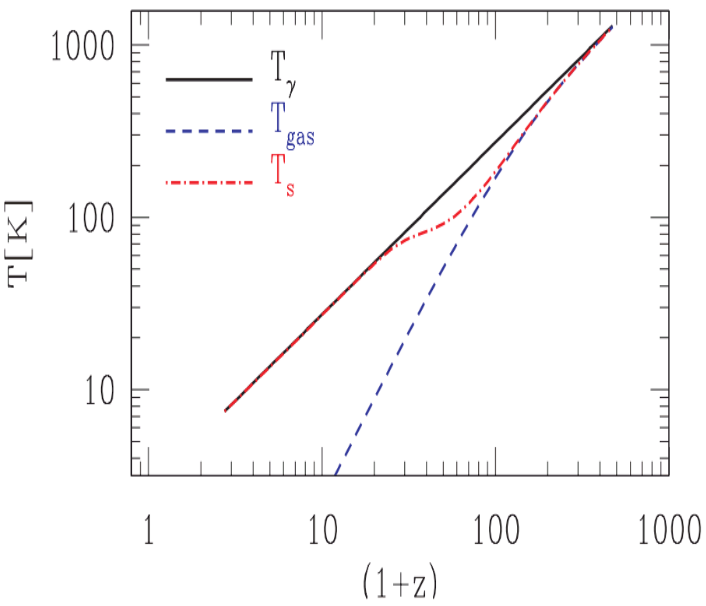

$$\frac{n_1}{n_0} = \frac{g_1}{g_0} e^{-T_\star/T_s}$$

$$T_b(\mathbf{n},\nu) = (T_s - T_\gamma)\,\tau/(1+z)$$

$$\boxed{T_b \propto (1 - T_\gamma/T_s)\, n_{\mathrm{H}}}$$

Redshifted HI 21-cm Signal

Dark ages ..

- Linear fluctuations
- HI is a tracer
- Gravitational wave imprint ?

Post reionization epoch..

- Absence of complex astrophysics
- HI again a biased tracer

  Investigate cross-correlations with other tracers

- CMBR anisotropies
  - CMBR ISW effect
  - CMBR Weak Lensing
- Lyman Alpha forest

scheme

The bias (with respect to the dark matter field) and the mean neutral fraction completely models the 21- signal in the post-reionization epoch

↓

Numerical Simulation of the 21-cm signal

(T. G. Sarkar, S Mitra, S. Majumdar, T. Roy Choudhury MNRAS 2012. arXiv : 1109.5552)

Bias model verified

↓

Observable Radio data → Power spectrum → Constraining Bias

Fisher Matrix – Principal Component Analysis

PARADIGM

HI IS A TRACER OF THE DARK MATTER FIELD

STATISTICS OF THE DARK MATTER FIELD

$\downarrow \quad \uparrow$

STATISTICS OF NEUTRAL GAS DISTRIBUTION

The bias (with respect to the dark matter field) and the mean neutral fraction completely models the 21- signal in the post-reionization epoch

Simulation :

608^3 particles in 1216^3 grids with grid spacing 0.1 Mpc in a 121.6 Mpc^3 box. The mass assigned to each dark matter particle is $m_{\rm part} = 2.12 \times 10^8 M_{\odot} h^{-1}$. The initial particle distribution and velocity field generated using Zel'dovich approximation

Friends-of-Friends algorithm (Davis et al. 1985) to identify dark matter over-densities as halos, taking linking length $b = 0.2$ (in units of mean inter-particle distance). This gives a reasonably good match with the theoretical halo mass function (Jenkins et al. 2001;

The neutral gas in halos can self shield itself from ionizing radiation only if the circular velocity is above a threshold of $v_{\rm circ} =$ 30km/sec at $z \sim 3$. This sets a lower cutoff for the halo mass $M_{\rm min}$. Further, halos are populated with gas in a way, such that the very massive halos do not contain any HI. An upper cut-off scale to halo mass $M_{\rm max}$ is chosen using $v_{\rm circ} = 200$km/sec, above which we do not assign any HI to halos. This is consistent with the observation that very massive halos do not contain any gas i

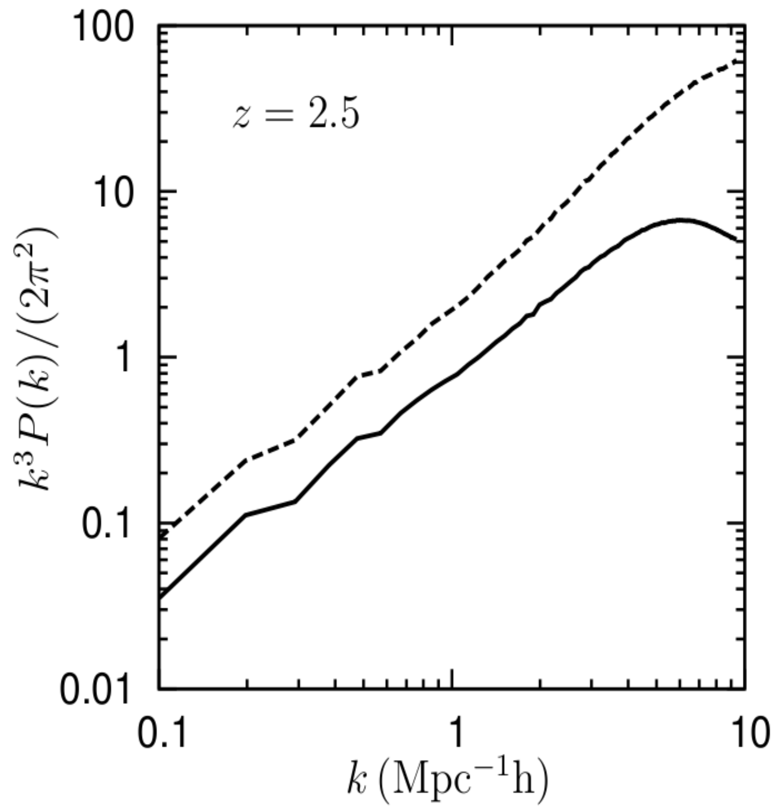

Figure 1. The simulated power spectra for dark matter distribution (solid line) and the HI density field (dashed line) at redshift $z = 2.5$.

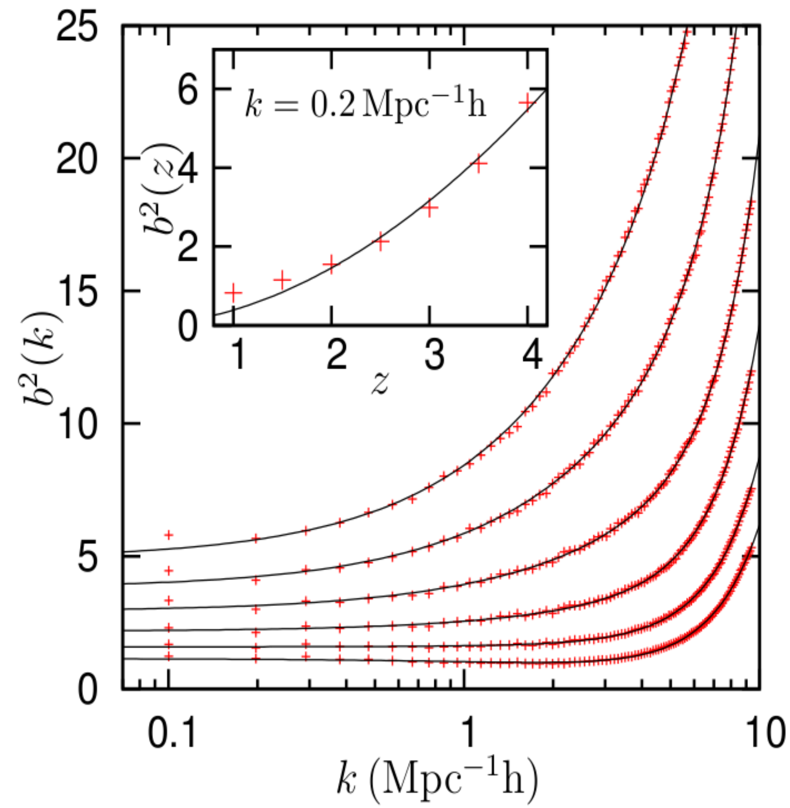

Figure 2. The simulated bias function for z =1.5, 2.0, 2.5, 3.0, 3.5 and 4.0 (bottom to top) showing the scale dependence. The inset shows the variation of the large-scale linear bias as a function of redshift.

T. G. Sarkar, S Mitra, S. Majumdar, T. Roy Choudhury (2011) MNRAS, 421, 4, pp. 3570-3578

Radio interferometric observation $\longrightarrow$ Cosmology

Measured Quantity : VISIBILITY

$$\mathcal{V}(\vec{U},\nu) = \mathcal{S}(\vec{U},\nu) + \mathcal{N}(\vec{U},\nu)$$

$$\mathcal{S}(\vec{U},\nu) = \int d^2\vec{\theta}\, A(\vec{\theta},\,\nu)\, I(\vec{\theta},\,\nu)\, e^{-i2\pi\vec{U}\cdot\vec{\theta}}$$

Fourier transform in the frequency direction yields

$$v(\vec{U}_a,\tau_m) = s(\vec{U}_a,\tau_m) + n(\vec{U}_a,\tau_m)$$

$$\langle s(\vec{U}_a,\tau_m)s^*(\vec{U}_b,\tau_n)\rangle = \frac{B\delta_{m,n}}{L^2r^2r'}\sum_{\vec{U}'}\tilde{A}(\vec{U}_a-\vec{U}')\tilde{A}^*(\vec{U}_b-\vec{U}')P_I(k'_\perp,k_{\parallel m})$$

ASTROPHYSICAL FOREGROUNDS SEVERAL ORDERS HIGHER

Lyman – α Forest as a cosmological probe

The redshifted light from a distant Quasar as it passes through the predominantly ionized IGM is absorbed when the redshifted frequency matches the Ly-alpha frequency in the rest frame of the neutral gas.

Small density fluctuations in the predominantly ionized IGM leads to A series of absorption peaks

Lyman – α Forest as a cosmological probe

The redshifted light from a distant Quasar as it passes through the predominantly ionized IGM is absorbed when the redshifted Frequency matches the Ly-alpha frequency in the rest frame of the neutral gas.

Small density fluctuations in the predominantly ionized IGM leads to A series of absorption peaks

Fluctuating GUNN-PETERSON EFFECT

- **Gas follows the dark matter**
- **Equilibrium leads to a power law temperature density relation**

Lyman – α Forest as a cosmological probe

The redshifted light from a distant Quasar as it passes through the predominantly ionized IGM is absorbed when the redshifted Frequency matches the Ly-alpha frequency in the rest frame of the neutral gas.

Small density fluctuations in the predominantly ionized IGM leads to A series of absorption peaks

High resolution (FWHM 6.6 km s-1) spectrum of the z = 3.62 QSO 1422+23 (V = 16.5), taken with the Keck HIRES (signal-to-noise ratio ~ 150 per resolution element, exposure time 25000 s). Womble et al (1996).

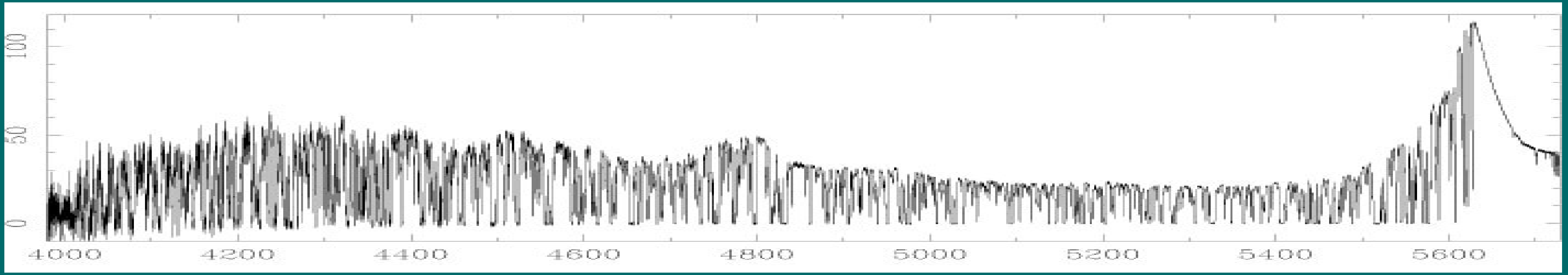

The fluctuations in the transmitted flux hence is believed to be a 1D probe of the underlying density field

The use of Lyman alpha forest as a cosmological probe has been studied in great details

Bi & Davidsen, 1997; Croft et al., 1998, 1999; Viel et al., 2002; Saitta et al., 2008

Traditional Cuisine !

Gunn & Peterson, 1965; Bi & Davidsen, 1997; Croft et al., 1998,

Traditional Cuisine !

One quantifies the Ly- α Flux fluctuations as

$$\delta_{\mathcal{F}}(\hat{\mathbf{n}}, z) = \mathcal{F}(\hat{\mathbf{n}}, z)/\bar{\mathcal{F}} - 1$$

The Fluctuating Gunn Peterson effect relates flux t

$$\mathcal{F} = \exp[-A(1+\delta)^{\kappa}]$$

Where A and k are two redshift dependent functio

On large scales Flux is proportional to matter over der

We may write

$$\boxed{\delta_\alpha(\hat{\mathbf{n}}, z) = C_\alpha \int \frac{d^3\mathbf{k}}{(2\pi)^3} e^{i\mathbf{k}.\hat{\mathbf{n}}r} [1 + \beta_\alpha \mu^2] \Delta(\mathbf{k})}$$

Redshift space distortion

where $\alpha = \mathcal{F}, T$ refers to the Ly-α flux and 21-cm brightness temperature

(McDonald, 2003) (Bagla et al., 2009)

<u>3D </u>Lyman – α Forest

Uses the full 3D information

Simulation of 3D flux power, relative to real-space linear theory (McDonald 2003)

Cross correlation of Lyman alpha forest with 21 cm

Guha Sarkar etal. (2011) MNRAS, Volume 410, Issue 2, pp. 1130-1134

$$\rho(\vec{\theta}) = \frac{\sum_a w_a \; \delta_D^2(\vec{\theta} - \vec{\theta}_a)}{\sum_a w_a}$$

$$\rho(\vec{\theta})\, \delta_{\mathcal{F}\mathrm{N}}(\vec{\theta}, n) = \frac{\sum_a w_a \; \delta_D^2(\vec{\theta} - \vec{\theta}_a) \; \delta_{\mathcal{F}\mathrm{N}}(\vec{\theta}_a, n)}{\sum_a w_a}$$

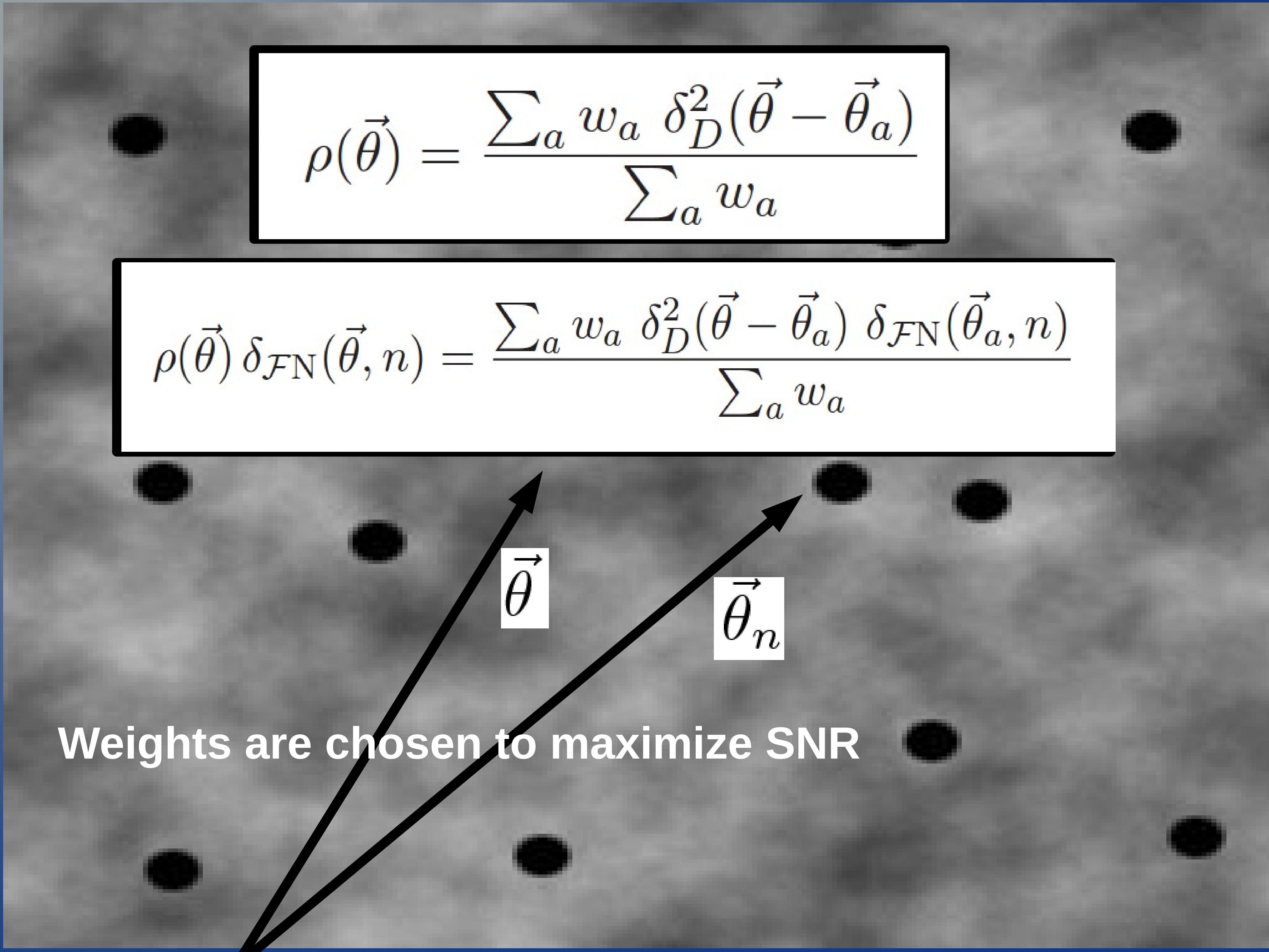

Weights are chosen to maximize SNR

Cross correlation of Lyman alpha forest with 21 cm

(angular power spectrum)

Guha Sarkar etal. (2011) MNRAS, Volume 410, Issue 2, pp. 1130-1134

Cross correlation in 3D

Late time cosmological evolution
Baryon Acoustic Oscillations

Early Universe
Primordial non Gaussianity

It is now well established that DARK ENERGY accounts for the lion's share of the Universe's matter budget

The ONLY way perhaps to “SEE” dark energy is through its imprint on the expansion history of the Universe

For Universe governed by Einstein's equation we have

$$H^2(z) = \frac{8\pi G}{3} \sum_i \rho_i(z)$$

The Probes :

- **Standard candles : OBJECTS OF KNOWN LUMINOSITY**
  - **measure d_L which is an integral of H^{-1}**
- **Standard rulers : OBJECTS OF KNOWN LENGTH**
  - **measure D_A [integral of $H^{-1}(z)$ and $H(z)$]**
- **Growth of fluctuations :**
  - **Crucial for testing extra ρ components vs modified gravity.**

STANDARD RULERS

If we knew the LENGTH OF A STANDARD OBJECT as a function of cosmic epoch

By noting the angle subtended by this ruler as a function of redshift we map the Angular diameter distance

$$\Delta\theta = \frac{\Delta\chi}{d_A(z)}$$

$$d_A(z) = \frac{d_L(z)}{(1+z)^2} \propto \int_0^z \frac{dz'}{H(z')}$$

And by measuring the redshift interval associated with this length we map out the Hubble parameter.

$$c\Delta z = H(z)\ \Delta\chi$$

WHERE DO WE FIND SUCH A RULER ???

Baryon Acoustic Oscillations

Cosmological density perturbations drive sound waves in the baryon
Photon plasma which are frozen once recombination takes place at
Z ~ 1000 leaving distinct oscillatory signature in the CMBR anisotropy

Prior to recombination photons and baryons were tightly coupled
A sudden recombination decouples the photons from the baryons
Giving a snap shot of the universe at the large scattering surface

$$(\Delta T)^2_{\mathrm{ls}} \sim \cos^2(k c_s t_{\mathrm{ls}}) + \text{velocity terms}$$

BAO also contributes imprints on the late time clustering of matter
However the effect is suppressed by a factor
Ω_b/Ω_m ~ 0.1

Baryon Acoustic Oscillations

http://astro.berkeley.edu/~mwhite/bao/

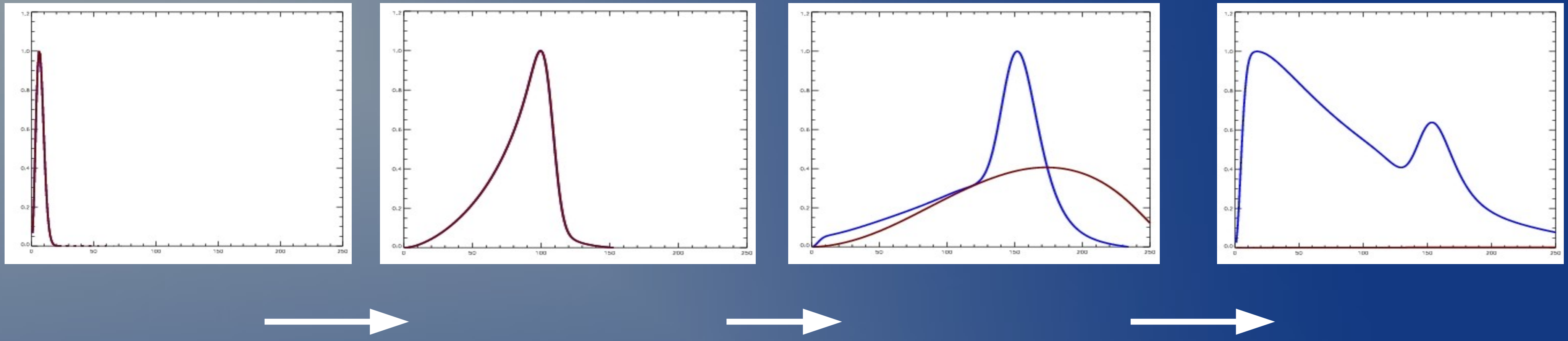

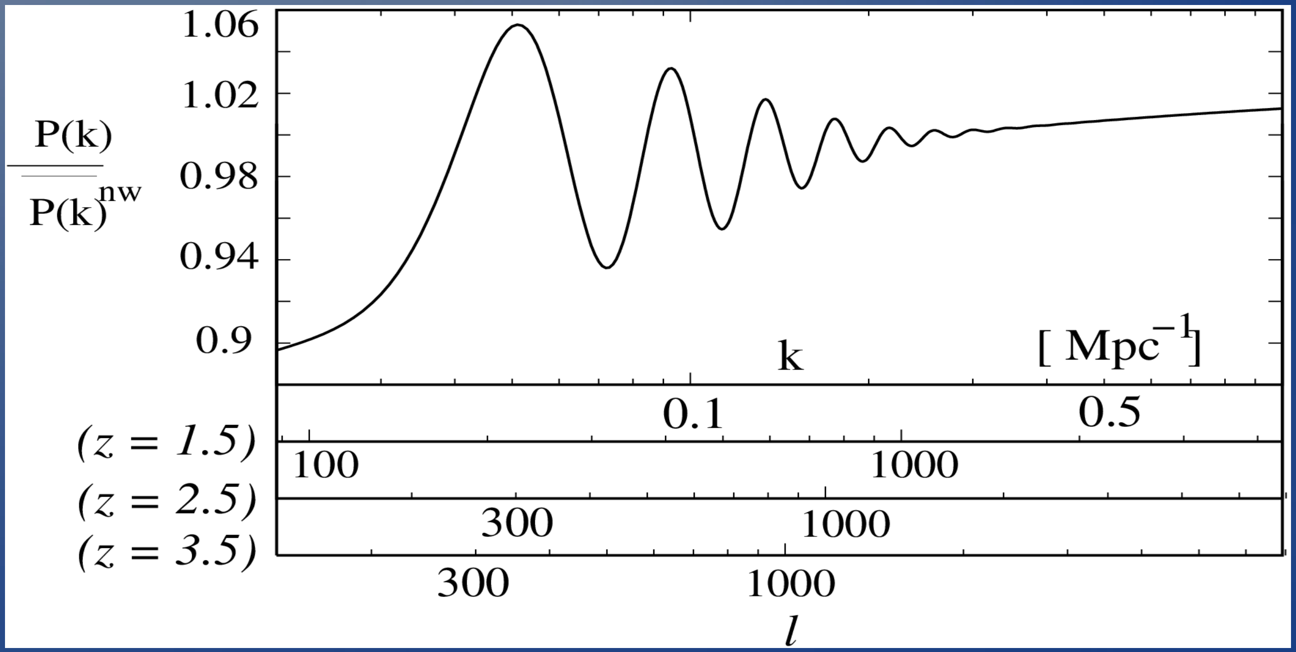

power spectrum (Eisenstein & Hu, 1998). The corresponding ℓ values have been shown for $z = 1.5, 2.5$ and 3.5.

$$F_{ij} = \frac{V}{(2\pi)^3} \int \frac{d^3\mathbf{k}}{[\mathcal{P}^2_{\mathcal{F}T}(\mathbf{k}) + \mathcal{P}_{\mathcal{F}\mathcal{F}o}(\mathbf{k})\mathcal{P}_{TTo}(\mathbf{k})]} \frac{\partial \mathcal{P}_{\mathcal{F}T}(\mathbf{k})}{\partial q_i} \frac{\partial \mathcal{P}_{\mathcal{F}T}(\mathbf{k})}{\partial q_j}$$

$$q_1 = \ln(s_\perp^{-1}) \text{ and } q_2 = \ln(s_\parallel)$$

$$D_V(z)^3 = (1+z)^2 D_A(z) \frac{cz}{H(z)}$$

$$\delta q_i = \sqrt{F^{-1}_{ii}}$$

$$\delta D_V / D_V = \tfrac{1}{3}(4F^{-1}_{11} + 4F^{-1}_{12} + F^{-1}_{22})^{0.5}$$

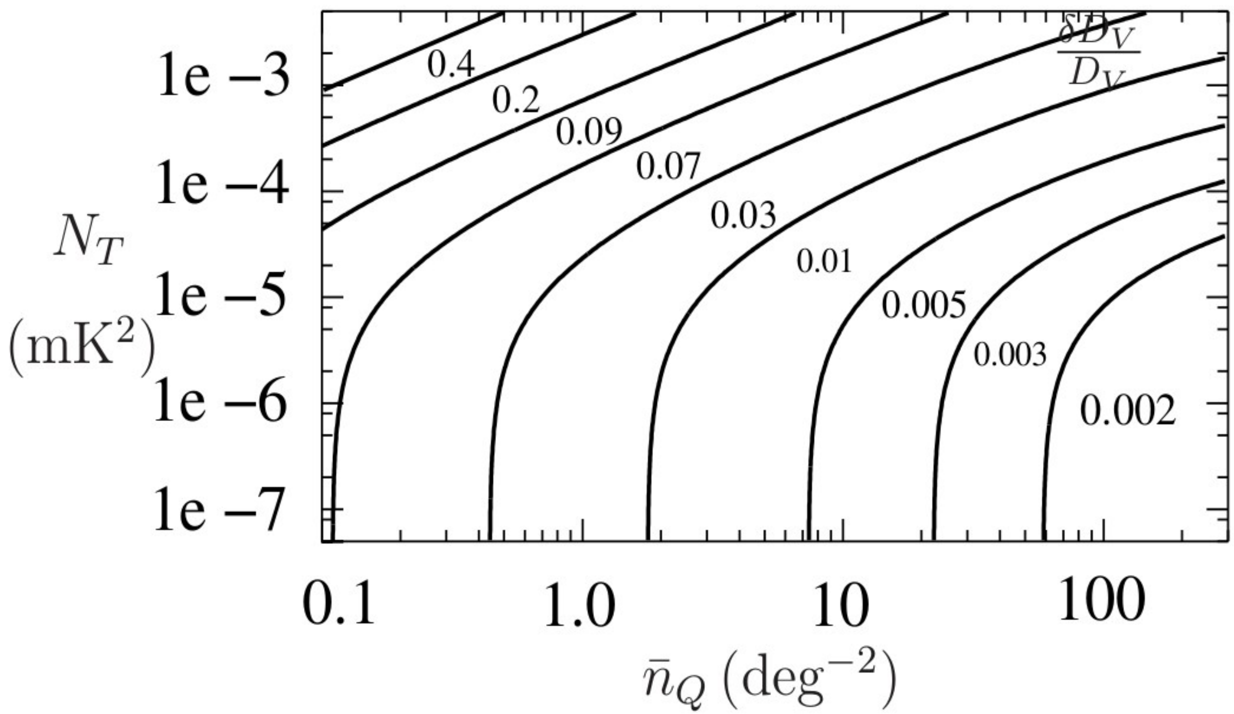

$$N_T = 1.0 \times 10^{-3}\,[m\mathrm{K}]^2 \left(\frac{500}{N_{ann}}\right)^2 \left(\frac{100\,\mathrm{KHz}}{\Delta\nu_c}\right) \left(\frac{1000\,\mathrm{hrs}}{\Delta t}\right)$$

Guha Sarkar T, Bharadwaj S, (2013)

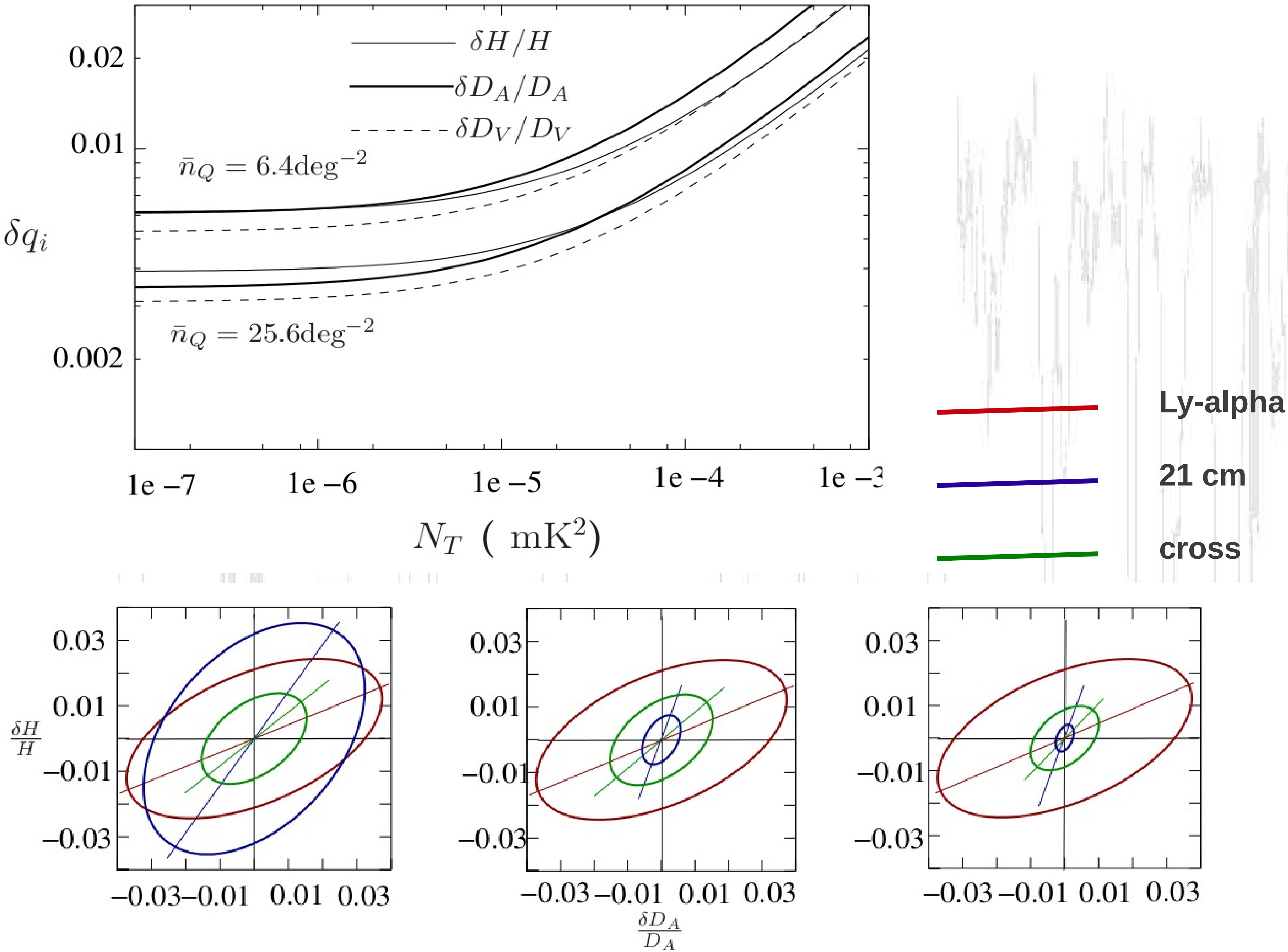

$\delta H/H$
$\delta D_A/D_A$
$\delta D_V/D_V$
$\bar{n}_Q = 6.4\mathrm{deg}^{-2}$
$\bar{n}_Q = 25.6\mathrm{deg}^{-2}$
δq_i
0.02
0.01
0.002
1e −7
1e −6
1e −5
1e −4
1e −3
N_T (mK^2)
Ly-alpha
21 cm
cross
$\frac{\delta H}{H}$
0.03
0.01
−0.01
−0.03
−0.03 −0.01 0.01 0.03
$\frac{\delta D_A}{D_A}$

Primordial non-Gaussianity

1D bispectrum of Lyman alpha forest
(Viel, Branchini, Dolag, Grossi, Matarrese, Moscardini, 2009, MNRAS, 393, 774)

3D bispectrum of Lyman alpha forest
(Hazra, Guha Sarkar, 2012 Phys. Rev. Lett. 109, 121301

3D cross-bispectrum of Lyman alpha forest and 21-cm
(Guha Sarkar, Hazra, 2012 Phys. Rev. Lett. 109, 121301

Non Gaussianity parameter is introduced through

$$\boxed{\Phi^{\rm prim} = \phi_G + \frac{f_{\rm NL}}{c^2}\left(\phi_G{}^2 - \langle\phi_G{}^2\rangle\right).}$$

We define the Power spectrum and Bispectrum as

$$\langle\Delta_{\mathbf{k}_1}\Delta_{\mathbf{k}_2}\rangle = \delta_D(\mathbf{k}_1+\mathbf{k}_2)P(k_1)$$

$$\langle\Delta_{\mathbf{k}_1}\Delta_{\mathbf{k}_2}\Delta_{\mathbf{k}_3}\rangle = \delta_D(\mathbf{k}_1+\mathbf{k}_2+\mathbf{k}_3)B(k_1,k_2,k_3)$$

Bispectrum from Primordial non-Gaussianity

$$\boxed{B^{\mathrm{L}}{}_{123} = \mathcal{M}(k_1)\mathcal{M}(k_2)\mathcal{M}(k_3)B_{\phi G\,123}}$$

Where $\mathcal{M}(k,z) = -\frac{3}{5}\frac{k^2 T(k)}{\Omega_m H_0^2}D_+(z)$ and

$$B_{\phi G\,123} = \frac{2f_{\mathrm{NL}}}{c^2}\left[P_{\phi G}(k_1)P_{\phi G}(k_2) + \mathrm{cyc}\right] + \mathcal{O}(f_{\mathrm{NL}}^3).$$

Bispectrum from non linear structure formation

Scoccimarro, Sefusatti, Zaldarriaga (2004)

$$\boxed{B_{123}^{\mathrm{NL}} = 2F_2(\mathbf{k}_1,\mathbf{k}_2)P(k_1)P(k_2) + \mathrm{cyc.}}$$

Finally $$\boxed{B_{123} = B_{123}^{\mathrm{L}} + B_{123}^{\mathrm{NL}}}$$

$$\delta_{\mathcal{F}} = \left(\mathcal{F}/\bar{\mathcal{F}} - 1\right)$$
$$\delta_{\mathcal{F}} = b_1\delta + \tfrac{1}{2}b_2\delta^2$$

$$\begin{aligned} P_{\mathcal{F}}(k) &= b_1^2 P(k) \\ \mathcal{B}_{\mathcal{F}123} &= b_1^3 B_{123} + b_1^2 b_2 \left[P(k_1)P(k_2) + \text{cyc.}\right] \end{aligned}$$

$$\delta_{\mathcal{F}} = \left(\mathcal{F}/\bar{\mathcal{F}} - 1\right)$$
$$\delta_{\mathcal{F}} = b_1 \delta + \tfrac{1}{2} b_2 \delta^2$$

$$\begin{aligned} P_{\mathcal{F}}(k) &= b_1^2 P(k) \\ \mathcal{B}_{\mathcal{F}123} &= b_1^3 B_{123} + b_1^2 b_2 \left[P(k_1)P(k_2) + \text{cyc.}\right] \end{aligned}$$

Desjacques, Seljak (2010);
Scoccimarro, Sefusatti, Zaldarriaga (2004)

$$\hat{\mathcal{B}}_{\mathcal{F}123} = \frac{V_f}{V_{123}} \int_{k_1} d^3\mathbf{q}_1 \int_{k_2} d^3\mathbf{q}_2 \int_{k_3} d^3\mathbf{q}_3 \delta_D(\mathbf{q}_{123}) \times \Delta^o_{\mathcal{F}}(k_1)\Delta^o_{\mathcal{F}}(k_2)\Delta^o_{\mathcal{F}}(k_3)$$

With

$V_f = (2\pi)^3/V$ And $V_{123} = \int_{k_1} d^3\mathbf{q}_1 \int_{k_2} d^3\mathbf{q}_2 \int_{k_3} d^3\mathbf{q}_3 \delta_D(\mathbf{q}_{123})$

$$F_{ij} = \sum_{k_1=k_{min}}^{k_{max}} \sum_{k_2=k_{min}}^{k_1} \sum_{k_3=\tilde{k}_{min}}^{k_2} \frac{1}{\Delta\hat{\mathcal{B}_{\mathcal{F}}}^2} \frac{\partial \mathcal{B}_{\mathcal{F}123}}{\partial p_i} \frac{\partial \mathcal{B}_{\mathcal{F}123}}{\partial p_j} \qquad \tilde{k}_{min} = max(k_{min}, |k_1 - k_2|)$$

$$\Delta\hat{\mathcal{B}_{\mathcal{F}}}^2 = \langle \hat{\mathcal{B}_{\mathcal{F}}}^2 \rangle - \langle \hat{\mathcal{B}_{\mathcal{F}}} \rangle^2. \qquad \Delta\hat{\mathcal{B}_{\mathcal{F}}}^2 = \frac{V_f}{V_{123}} s P_{\mathcal{F}}^{\mathrm{Tot}}(k_1) P_{\mathcal{F}}^{\mathrm{Tot}}(k_2) P_{\mathcal{F}}^{\mathrm{Tot}}(k_3) \qquad s = 6, 1$$

$$P_{\mathcal{F}}^{\mathrm{Tot}}(\mathbf{k}) = P_{\mathcal{F}}(\mathbf{k}) + P_{\mathcal{F}}^{\mathrm{1D}}(k_{||}) P_W + N_{\mathcal{F}}$$

$$F_{ij} = \sum_{k_1=k_{min}}^{k_{max}} \sum_{k_2=k_{min}}^{k_1} \sum_{k_3=\tilde{k}_{min}}^{k_2} \frac{1}{\Delta\hat{\mathcal{B}_{\mathcal{F}}}^2} \frac{\partial \mathcal{B}_{\mathcal{F}123}}{\partial p_i} \frac{\partial \mathcal{B}_{\mathcal{F}123}}{\partial p_j}$$

$$\tilde{k}_{min} = max(k_{min}, |k_1 - k_2|)$$

$$\Delta\hat{\mathcal{B}_{\mathcal{F}}}^2 = \langle \hat{\mathcal{B}_{\mathcal{F}}}^2 \rangle - \langle \hat{\mathcal{B}_{\mathcal{F}}} \rangle^2. \quad \Delta\hat{\mathcal{B}_{\mathcal{F}}}^2 = \frac{V_f}{V_{123}} s P_{\mathcal{F}}^{\mathrm{Tot}}(k_1) P_{\mathcal{F}}^{\mathrm{Tot}}(k_2) P_{\mathcal{F}}^{\mathrm{Tot}}(k_3) \qquad s = 6, 1$$

$$P_{\mathcal{F}}^{\mathrm{Tot}}(\mathbf{k}) = P_{\mathcal{F}}(\mathbf{k}) + P_{\mathcal{F}}^{\mathrm{1D}}(k_{||}) P_W + N_{\mathcal{F}}$$

For high SNR spectra $\qquad P_W = \frac{1}{\bar{n}}$

Equilateral configuration

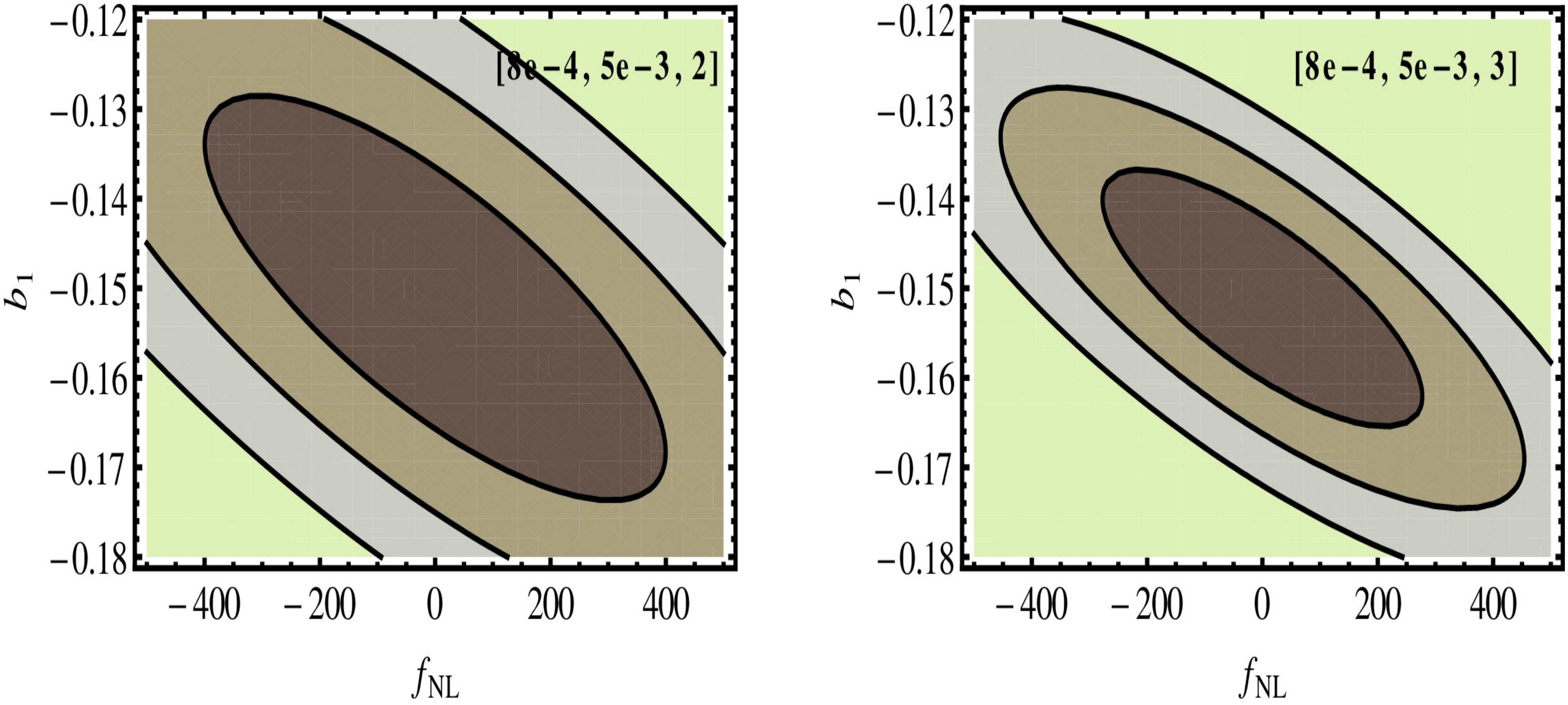

D. Hazra, T. Guha Sarkar, Phys. Rev. Lett. 109, 121301 (2012)

k_{min} (Mpc^{-1})	$\bar{n}$ (Mpc^{-2})	S/N	Δf_{NL}	Δb_1
2×10^{-3}	2.2×10^{-3}	5	228.84	1.1×10^{-2}
1×10^{-3}	2.2×10^{-3}	5	161.81	7.7×10^{-3}
5×10^{-4}	2.2×10^{-3}	5	114.42	5.5×10^{-3}
8×10^{-4}	1.0×10^{-3}	5	272.95	1.5×10^{-2}
8×10^{-4}	2.2×10^{-3}	5	144.73	6.9×10^{-3}
8×10^{-4}	5.0×10^{-3}	5	91.65	3.5×10^{-3}
8×10^{-4}	2.2×10^{-3}	2	263.52	1.5×10^{-2}
8×10^{-4}	2.2×10^{-3}	3	182.83	9.5×10^{-3}
8×10^{-4}	2.2×10^{-3}	4	156.56	7.7×10^{-3}
Ideal case				
5×10^{-4}	1	5	23.72	2.1×10^{-4}

TABLE I: The bounds on (f_{NL}, b_1) obtained from Fisher analysis for various combinations of (k_{min}, $\bar{n}$, S/N).

D. Hazra, T. Guha Sarkar, Phys. Rev. Lett. 109, 121301 (2012)

Cross – bispectrum of Ly-alpha forest and redshifted 21-cm signal
(T. Guha Sarkar, D. Hazra, (2012))

Consider two tracer fields *R* and *S*

$$R(\mathbf{k})\,[S(\mathbf{k})] = b^{(1)}_{\mathrm{R[S]}}\Delta(\mathbf{k}) + \frac{b^{(2)}_{\mathrm{R[S]}}}{2}\Delta(\mathbf{k})^2$$

$$\begin{aligned} P_{RS}(k) &= b^{(1)}_{\mathrm{R}} b^{(1)}_{\mathrm{S}} P(k) \\ \mathcal{B}_{RSS} &= \frac{b^{(1)}_{\mathrm{R}} {b^{(1)}_{\mathrm{S}}}^2}{3}\left[B_{123} + B_{231} + B_{312}\right] + \frac{1}{3}\Big[2 b^{(1)}_{\mathrm{R}} b^{(1)}_{\mathrm{S}} b^{(2)}_{\mathrm{S}} \left(P(k_1)P(k_2) + \mathrm{cyc.}\right) \\ &+ b^{(2)}_{\mathrm{R}} b^{(1)}_{\mathrm{S}} b^{(1)}_{\mathrm{S}} \left(P(k_1)P(k_2) + \mathrm{cyc.}\right)\Big]. \end{aligned}$$

$$\Delta\hat{\mathcal{B}}_{RSS}{}^2 = \frac{V_f}{9V_{123}}\left[t\left(P^{\mathrm{Tot}}_{\mathrm{R}}(k_1)P^{\mathrm{Tot}}_{\mathrm{S}}(k_2)P^{\mathrm{Tot}}_{\mathrm{S}}(k_3) + \mathrm{cyc.}\right) + 2t\left(P^{\mathrm{Tot}}_{\mathrm{S}}(k_1)P^{\mathrm{Tot}}_{\mathrm{RS}}(k_2)P^{\mathrm{Tot}}_{\mathrm{RS}}(k_3) + \mathrm{cyc.}\right)\right]$$

21 -cm observation using a SKA like radio array

406 MHz corresponding to $z = 2.5$

area of 45 m^2 (fov $\sim \pi 8.6^2 \mathrm{deg}^2$)

1400 antennas

total observing time of 4000 hrs.

Lyman alpha survey (10, 000 sq deg)

$$\bar{n} = 10^{-3}\ \mathrm{Mpc}^{-2}$$

S/N = 2 for 1Å pixels.

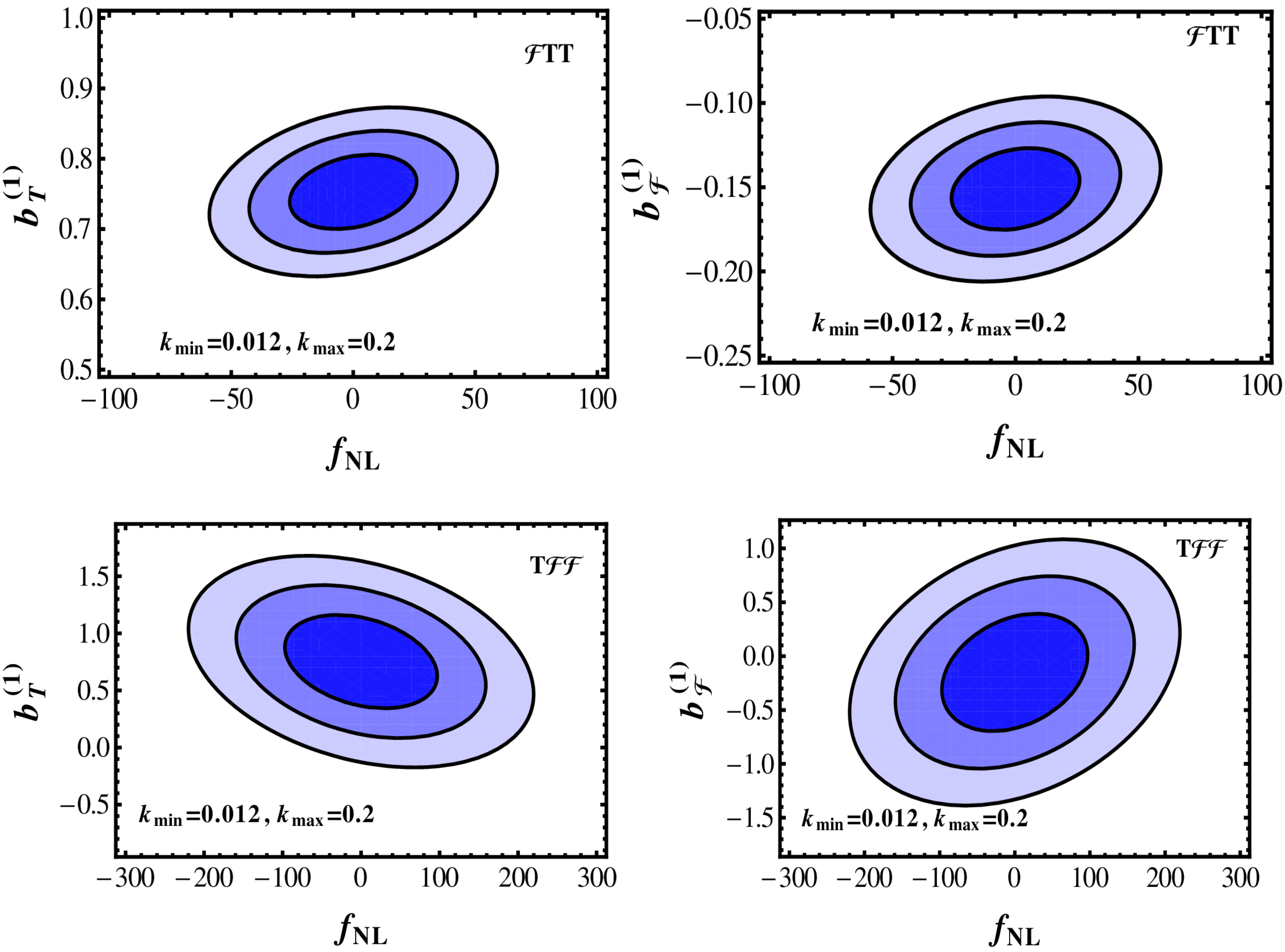

$\mathcal{F}$TT
$k_{\min}=0.012$, $k_{\max}=0.2$
$b_T^{(1)}$
f_{NL}
$\mathcal{F}$TT
$k_{\min}=0.012$, $k_{\max}=0.2$
$b_{\mathcal{F}}^{(1)}$
f_{NL}
T$\mathcal{F}\mathcal{F}$
$k_{\min}=0.012$, $k_{\max}=0.2$
$b_T^{(1)}$
f_{NL}
T$\mathcal{F}\mathcal{F}$
$k_{\min}=0.012$, $k_{\max}=0.2$
$b_{\mathcal{F}}^{(1)}$
f_{NL}

Estimator	$\mathcal{F}\mathcal{F}\mathcal{F}$	$\mathrm{T}\mathcal{F}\mathcal{F}$	$\mathcal{F}\mathrm{TT}$	TTT
Parameters	$p_2 = b_{\mathcal{F}}^{(1)}$ $p_3 = b_{\mathcal{F}}^{(2)}$	$p_2 = b_{\mathrm{T}}^{(1)}$ $p_3 = b_{\mathcal{F}}^{(1)}$	$p_2 = b_{\mathrm{T}}^{(1)}$ $p_3 = b_{\mathcal{F}}^{(1)}$	$p_2 = b_{\mathrm{T}}^{(1)}$ $p_3 = b_{\mathrm{T}}^{(2)}$
Δf_{NL}	9.4	64	17.2	6.3
Δp_2	7×10^{-4}	0.28	3.5×10^{-2}	1.4×10^{-3}
Δp_3	3×10^{-3}	0.36	2×10^{-2}	4×10^{-3}
r_{12}	4×10^{-3}	-0.31	0.27	0.2
r_{13}	-0.21	0.3	0.21	0.22
r_{23}	-0.93	-0.99	0.99	-0.86

T. Guha Sarkar, D. Hazra, (2012) arXiv :1211.4756

Thank you